MALAYSIAN JOURNAL OF MICROSCOPY

Journal homepage: https://malaysianjournalofmicroscopy.org

RESEARCH ARTICLE

FAILURE ANALYSIS OF NATURAL GAS FUEL SUPPLY TUBES IN POWER PLANT COMBUSTION SYSTEMS

Shaiful Rizam Shamsudin[1,*], Wan Mohd Haqqi Wan Ahmad[2], Mohd Rafi Adzman[3], Murizam Darus[1], Ruhiyuddin Mohd Zaki[2], Nur Farhana Hayazi[2], Jafri Kassim[1]

[1]Faculty of Mechanical Engineering & Technology, Universiti Malaysia Perlis, 02600 Arau, Perlis, Malaysia.
[2]Faculty of Chemical Engineering & Technology, Universiti Malaysia Perlis, 02600 Arau, Perlis, Malaysia.
[3]Faculty of Electrical Engineering & Technology, Universiti Malaysia Perlis, 02600 Arau, Perlis, Malaysia.

Abstract. Failures in natural gas fuel supply systems are often linked to the combined effects of material degradation, operational factors, and improper installation practices. In this study, the primary cause was identified as an installation error at the tube bend, leading to condensation-induced corrosion. Rapid temperature and pressure fluctuations during shutdowns created ideal conditions for moisture accumulation, particularly at the bend, which accelerated corrosion. The failure mechanisms involved stress corrosion cracking (SCC), sulfide stress cracking (SSC), hydrogen embrittlement (HE), and localised pitting corrosion. The presence of hydrogen sulfide (H_2S) and trace amounts of chlorides in the natural gas further intensified the degradation. The methodology included visual inspection, chemical composition analysis, stereomicroscopy, optical microscopy, scanning electron microscopy (SEM), and energy-dispersive spectroscopy (EDS). These analyses identified the extent of condensation-induced corrosion and the failure points. Results confirmed that the tube bend geometry contributed to moisture retention, exacerbating the corrosion process. Although AISI 304 stainless steel is suitable for general applications, it performs poorly in environments with moisture and condensation, as these promote passive film breakdown. Rapid temperature and pressure drops during shutdowns enhanced moisture condensation and corrosion under the influence of corrosive gases. The discussion highlights the need to redesign the tube bend geometry, adopt corrosion-resistant materials such as AISI 316L or AISI 321 stainless steel, and implement stress-relief and inspection techniques. Addressing the installation error, material selection, and operational practices will help prevent future failures and ensure long-term performance.

Keywords: Stress corrosion cracking, sulfide stress cracking, hydrogen embrittlement, condensation-induced corrosion, stainless steel.

Article Info

Received 28 January 2025
Accepted 8 October 2025
Published 4 December 2025

***Corresponding author: rizam@unimap.edu.my**

ISSN: 1823-7010, eISSN: 2600-7444

1. INTRODUCTION

Corrosion-induced failures in natural gas systems pose significant safety and operational challenges, especially in high-pressure and high-temperature environments. These failures can reduce plant reliability, raise maintenance costs, and cause unplanned shutdowns or hazardous gas leaks. Among various corrosion mechanisms, stress corrosion cracking (SCC) and sulfide stress cracking (SSC) are the most critical degradation modes in stainless steel components operating under mixed gaseous and condensate conditions. SCC is typically intensified by thermal cycling, residual stresses, and chloride contamination, while SSC develops under high-stress exposure to wet hydrogen sulfide (H_2S) [1]. Specifically, SSC results from hydrogen embrittlement, where atomic hydrogen generated during corrosion penetrates the metal lattice and weakens intergranular cohesion [2,3]. The presence of moisture further accelerates both mechanisms by facilitating hydrogen diffusion (in SSC) and electrolyte formation (in SCC), increasing vulnerability to hydrogen-induced cracking (HIC) [4]. Failures caused by these processes in natural gas pipelines and fuel systems have led to severe safety, environmental, and economic consequences, particularly in ageing infrastructure or systems with insufficient maintenance [5].

The corrosion behavior of fuel supply tubing systems becomes more complex under intermittent operation and cyclic pressure–temperature conditions. During startup and shutdown cycles, rapid temperature fluctuations generate steep thermal gradients that induce residual stresses [6]. Moisture condensation during shutdowns produces localised wet zones where dissolved gases such as CO_2 and H_2S form weak acids, destabilizing the passive oxide film of stainless steels [4,7]. Once the film is damaged, localised attacks like pitting or crevice corrosion occur, creating potential initiation sites for SCC [8-12]. Under these cyclic and chemically aggressive conditions, the combined effects of mechanical stress, condensate chemistry, and geometrical constraints often lead to premature failure of tubing components [10,13]. Stagnant condensate in low-lying sections further worsens local corrosion, while repeated pressurization and vibration accelerate crack propagation [8,14,15].

In coastal or humid environments, airborne chlorides intensify these effects. Chloride ions compromise the stability of the protective Cr_2O_3 layer on stainless steel, promoting localised corrosion even at low concentrations [1,11]. This condition is particularly relevant to Malaysian power plants, many of which are located near the coast and operate in tropical humidity [5]. The interaction between chloride-induced film breakdown, hydrogen ingress from H_2S exposure, and cyclic stress results in a synergistic deterioration mechanism that exceeds the protection capacity of conventional corrosion-resistant materials [6,7]. Hence, understanding the combined influence of condensate formation, environmental contaminants, and stress concentration under real plant conditions is essential for developing effective mitigation strategies.

A recent failure incident in a local combined-cycle power plant illustrates these issues. The plant operates in a 3-3-1 configuration (three gas turbines, three heat recovery steam generators, and one steam turbine) and experienced recurrent pressure drops and water buildup in its natural gas fuel supply tubes after about 25,000 operating hours. The affected tubes were made of 304L stainless steel, with a 16 mm outer diameter and 2 mm thickness, operating at 20–25 bar and 140 °C. Although 304L steel generally provides good corrosion resistance, it remains prone to SCC in chloride-rich conditions and SSC under H_2S exposure [1]. Thermal cycling during shutdowns worsens the situation: condensate forms carbonic acid that triggers localised corrosion, while rapid temperature changes induce thermo-mechanical fatigue, amplifying SCC and SSC susceptibility [6,7]. These combined degradation factors significantly reduce the structural integrity and lifespan of the tubing.

This study aims to identify the root causes of natural gas fuel tube failures in a combined-cycle plant by integrating metallurgical, chemical, and microstructural analyses with operational data. It establishes correlations between condensation-induced corrosion, hydrogen embrittlement, and stress mechanisms under real conditions, offering practical insights into how condensate, gas composition, and shutdown procedures influence degradation. The findings are expected to support better design, material selection, and operational strategies to prevent recurrence.

2. MATERIALS AND METHODS

A site visit was conducted during a scheduled plant shutdown to inspect and assess the condition of the failed natural gas fuel supply tubes within the gas turbine combustion system. During the inspection, visual observations were performed following a predefined protocol, and digital photographs were captured to document surface conditions, discolouration, deposits, or visible cracks. Leak detection was performed using a pneumatic pressure test combined with a soap bubble application, which effectively identified fine leak paths along welded and bent regions. Tubes showing leakage or surface damage were marked, removed from the system, and transported under controlled environmental conditions to prevent contamination during laboratory investigation.

Chemical composition analysis was performed using optical emission spectroscopy (OES) (Q8 Magellan, Bruker) to validate compliance with the standard specifications of AISI 304L stainless steel. Non-destructive testing (NDT) was carried out using liquid penetrant inspection (LPI) to identify and map surface-breaking flaws. For morphological analysis, a stereomicroscope (Leica S8 APO) was used to characterise macro-crack patterns and surface topography. High-resolution imaging and elemental analysis were performed using scanning electron microscopy (SEM) (Quanta 450, FEI) operated at 20 kV with a working distance of 10 mm and coupled with energy-dispersive X-ray spectroscopy (EDS) using a spot size of 1 µm. Metallographic preparation involved sectioning the tubes with a precision cutter, mounting them in epoxy resin, and performing sequential grinding using silicon carbide (SiC) abrasive papers (100, 240, 400, 600, and 1000 grit) under water lubrication. This was followed by polishing with diamond suspensions of 6 µm and 1 µm particle size. Samples were etched with freshly prepared aqua regia (nitric acid and hydrochloric acid in a 1:3 volume ratio) to reveal grain structure and crack morphology. Microstructural evaluations were conducted using an Olympus BX41 M optical microscope at magnifications of 50 to 500X to determine the presence of intergranular or transgranular cracking patterns.

3. RESULTS AND DISCUSSION

3.1 Site Visit, Visual Inspection and Dye Penetrant Test

Figure 1 shows camera photographs of the leak investigation. A site visit was conducted to assess the fuel gas supply tubes connected to the combustion system. Initial visual inspection (Figure 1(a)) revealed no visible leaks; however, a soap bubble test identified multiple leaks along the straight section near the bend (Figure 1(b)). The leaks were predominantly localised at the 6 o'clock position (Figure 1(c)), while the bend itself showed no visible defects. Dye Penetrant Inspection (DPI) confirmed surface-breaking flaws at these locations (Figure 1(d)).

The absence of leaks at the bend contrasts with typical SCC initiation at geometric stress concentrators, as observed by Radhakrishnan et al. [8]. Instead, leakage at the straight section aligns with gravitational water settling, as noted by Ajayi and Lyon [9], where stagnant condensate accelerates localised corrosion. Pitting corrosion is proposed as the primary failure initiator, as prolonged exposure to moisture and chloride diffusion likely caused passive film breakdown, creating sites for crack nucleation. This hypothesis is supported by EDS analysis (Section 3.4), which confirmed chloride and sulfur deposits at the failure sites.

While residual stress from thermal cycling may contribute to crack propagation, the dominance of localised pitting suggests SCC initiation was driven by environmental factors (moisture, chlorides) rather than mechanical stress alone. Secondary stressors, such as thermal expansion/ contraction cycles, may further exacerbate crack growth, warranting deeper investigation into their role in failure progression.

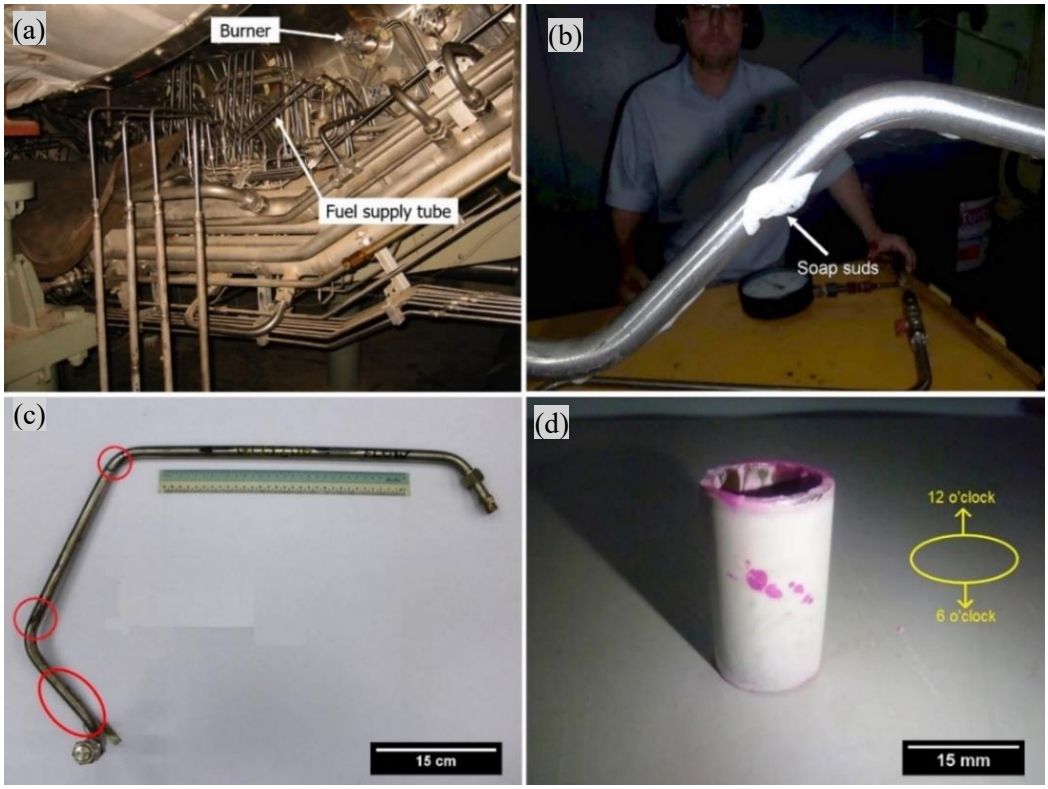

Figure 1: Camera photographs of the leak investigation: (a) Overall tube condition, (b) Soap bubble test, (c) Marked leak locations and (d) DPI confirming leakage at the 6 o'clock position

3.2 Chemical Composition

The chemical composition of natural gas, diesel, and the failed fuel supply tube was analysed to identify factors contributing to material degradation. As shown in Table 1, methane (CH_4) dominated the natural gas composition (91–92 vol.%), followed by ethane (C_2H_6, 5–6 vol.%) and propane (C_3H_8, 2 vol.%). Critical corrosive species included hydrogen sulfide (H_2S, 5–6 ppm) and hydrogen chloride (HCl, 2–2.5 ppm), which align with Elkhodbia et al. [10] in their identification of SSC and chloride-induced corrosion risks. Trace methyl chloride (CH_3Cl, 1–1.5 ppm) and ethyl chloride (C_2H_5Cl, 1–1.5 ppm) further elevate pitting susceptibility in stainless steel. The 0.02 vol.% water content, combined with CO_2, supports Fonseca et al.'s [11] findings that carbonic acid (H_2CO_3) may forms in the presence of condensate and CO_2 during shutdowns, accelerating passive film breakdown and localised corrosion.

Table 1: Chemical composition of natural gas

Compound	NG 1	NG 2
Methane (CH_4, vol.%)	92	91
Ethane (C_2H_6, vol.%)	5	6
Propane (C_3H_8, vol.%)	2	2
Butanes (C_4H_{10}, vol.%)	0.8	0.7
Carbon Dioxide (CO_2, vol.%)	0.7	0.8
Nitrogen (N_2, vol.%)	0.4	0.4
Hydrogen Sulfide (H_2S, ppm)	5 ppm	6
Hydrogen Chloride (HCl, ppm)	2	2.5
Methyl Chloride (CH_3Cl, ppm)	1	1
Ethyl Chloride (C_2H_5Cl, ppm)	1	1.5
Oxygen (O_2, vol.%)	0.05	0.05
Helium (He, vol.%)	0.05	0.05
Water (H_2O, vol.%)	0.02	0.02
Other Trace Gases	Trace	Trace

Table 2 reveals a diesel composition dominated by alkanes (73–75 vol.%), cycloalkanes (12–14 vol.%), and aromatics (10–11 vol.%). The relatively low sulfur content (0.04–0.05 wt.%) complies with modern ultra-low-sulfur fuel specifications, reducing the formation of corrosive SO_2 and H_2S during combustion. However, the presence of aromatic and olefinic compounds (1.5–2 vol.%) may still promote high-temperature oxidation, carbon deposition, and surface carburization under oxidising or catalytic conditions. Although the 0.02 wt.% water content appears minimal, it can condense in inactive flow regions and form micro-electrolytic cells, thereby accelerating pitting corrosion and hydrogen embrittlement (HE) in stagnant or thermally cycled metallic zones.

Table 2: Chemical composition of diesel

Compound	D 1	D 2
Alkanes (C_{14}–C_{18}), vol. %	75	73
Cycloalkanes, vol. %	12	14
Aromatics, vol.%	10	11
Olefinic Compounds, vol. %	2	1.5
Sulfur (S), wt. %	0.05	0.04
Oxygen (O_2), wt. %	0.03	0.04
Nitrogen (N_2), wt. %	0.01	0.01
Water (H_2O), wt. %	0.02	0.02
Ash, wt. %	0.01	0.01
Cetane Number	50	52

Table 3 shows the chemical composition of the failed tube sample. The failed tube, fabricated from AISI 304L stainless steel met compositional specifications with chromium (17.59 wt%) and nickel (9.65 wt%). However, minor sulfur (0.013 wt.%) and phosphorus (0.03 wt.%) levels—within ASTM A240 limits—could promote sulfide inclusions and localised corrosion in H_2S/ Cl^- environments. This aligns with Scatigno et al. [1], who linked sulfur-induced inclusions to pitting and micro-cracking under tensile stress. While the material is nominally compliant, cyclic thermal/ pressure stresses and corrosive gas exposure likely synergised to accelerate degradation.

Table 3: Chemical composition of failed sample

Element	Specimen	AISI 304L
C	0.026	0.0 - 0.03
Mn	1.285	0.0 - 2.00
P	0.03	0.0 - 0.05
S	0.013	0.0 - 0.02
Si	0.465	0.0 - 1.00
Cr	17.59	17.50 - 19.50
Ni	9.653	8.00 - 10.50
N	0.04	0.0 - 0.11
Fe	70.06	Balance

3.3 Macroscopic View

Stereomicroscope analysis revealed critical insights into the failure mechanism, with distinct crack patterns and corrosion damage observed on both external and internal tube surfaces (Figure 2). The outer surface (Figure 2(a)) exhibited a primary crack propagating diagonally at approximately 45°, accompanied by multiple secondary branching cracks along the grain boundaries. These morphological

features are characteristic of brittle fracture behaviour, often associated with high tensile stresses, low operating temperatures, or exposure to corrosive species that weaken the metal matrix, as reported by Yu et al. [12]. The presence of secondary cracks indicates localised stress concentration zones that accelerate corrosion penetration and structural weakening, consistent with observations by Alhede et al. [15].

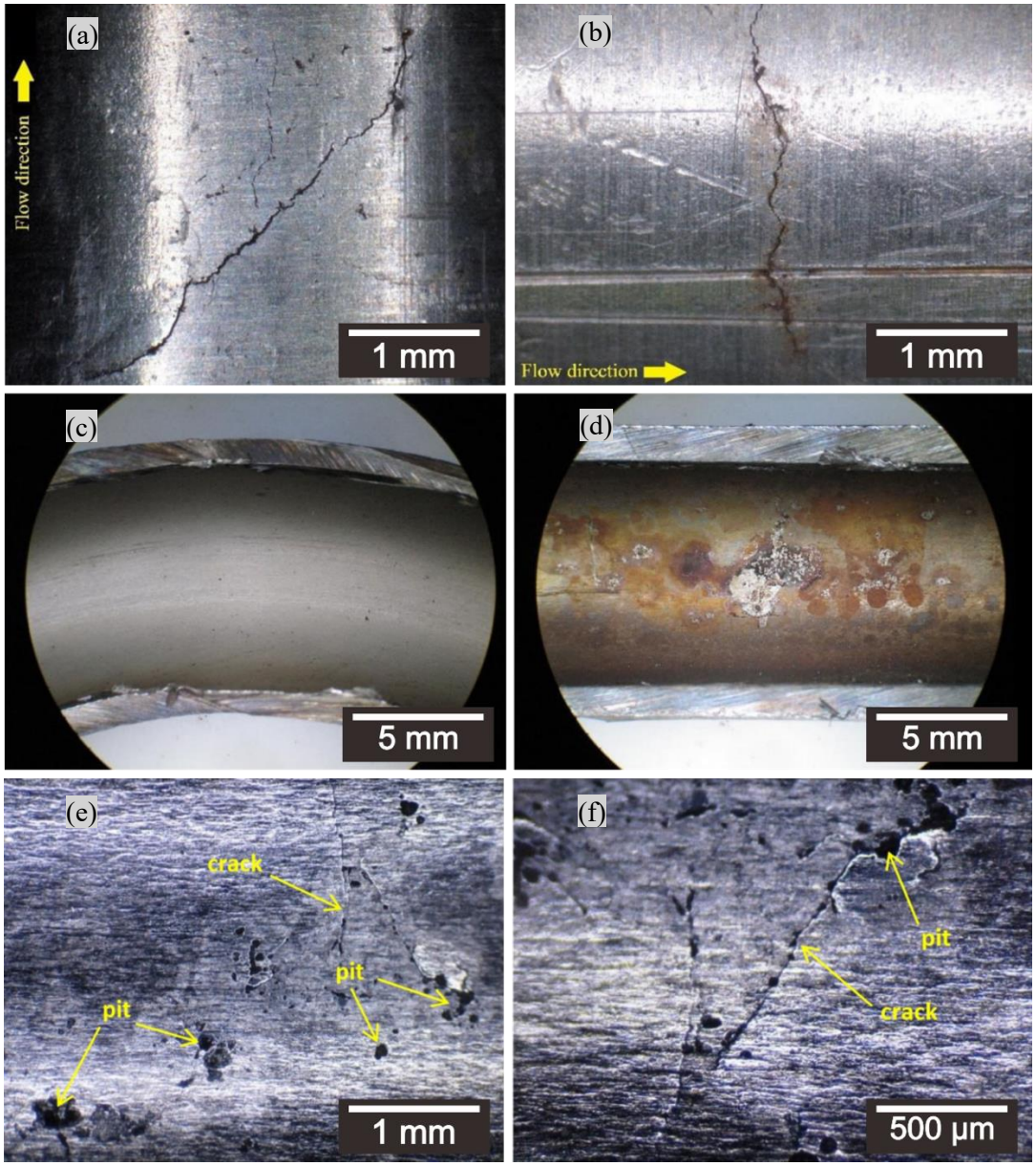

Figure 2: Stereomicroscope macrographs of the failed fuel supply tube showing (a) primary and secondary cracks, (b) a perpendicular crack, (c) a clean bent section, (d) rust at the 6 o'clock position, (e) pitting on the outer surface, and (f) pitting with cracks on the inner surface

SCC was evident, emphasising the role of tensile stresses in accelerating degradation in corrosive environments, as observed by Hamdan et al. [13]. The internal surface showed corrosion-driven damage, with aggressive species (e.g., chlorides and sulfide ions) weakening the passive film. The bent section (Figure 2(c)) appeared macroscopically defect-free, consistent with findings that bending did not induce visible damage. However, the straight section at the 6 o'clock position (Figure 2(d)) displayed brownish corrosion products, indicating a localised attack. Pitting corrosion was observed on both outer (Figure 2(e)) and inner (Figure 2(f)) surfaces, with cracks initiating near pits. This supports pitting as a precursor to structural failure, as pits act as stress concentrators for SCC. The

coexistence of brittle fracture and corrosion-driven damage underscores the need to assess both external and internal surfaces to ensure long-term tube integrity.

3.4 Presence of Corrosive Elements

Figure 3 presents EDS spectra from two regions of the failed fuel supply tube, providing insights into elemental composition and corrosion mechanisms. The EDS spectrum of the base metal (Figure 3(a)) shows dominant peaks for iron (Fe), chromium (Cr), and nickel (Ni), consistent with AISI 304 stainless steel composition. Minor oxygen (O) and carbon (C) signals suggest surface oxidation or contamination, aligning with Latypova & Latypov's [14] observations of similar surface phenomena in stainless steels. In contrast, the EDS spectrum of the corrosion deposits (Figure 3(b)) reveals Fe, Cr, and Ni, alongside notable sulfur (S) and oxygen (O) peaks, and a weak chlorine (Cl) signal. These elements are critical to corrosion mechanisms: Sulfur (S) indicates SSC, typically linked to hydrogen sulfide (H_2S) exposure in wet environments [11]. Whereas, chlorine (Cl^-), even at low concentrations, aligns with established links to pitting corrosion in stainless steels [1,10].

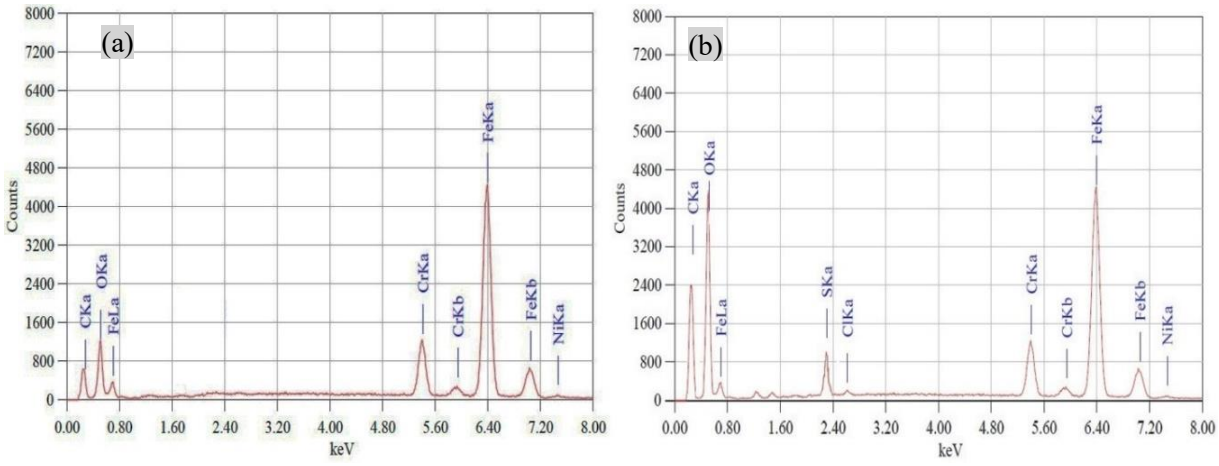

Figure 3: EDS patterns of the internal tube wall at (a) the unaffected bend and (b) the corroded straight section

The coexistence of S and Cl^- suggests a synergistic degradation mechanism, where H_2S promotes SSC while chlorides accelerate pitting and passive film breakdown. This aligns with prior studies linking material susceptibility (e.g., AISI 304's low molybdenum content) to localised corrosion in aggressive environments [1,10].

3.5 Microstructure on Leaked Location

Microstructural analysis was conducted to examine the crack propagation behaviour and the extent of material degradation in the failed natural gas fuel supply tube. Figure 4 presents a comparative evaluation of both as-polished and etched microstructures, revealing critical evidence of the underlying failure mechanisms and their progression over time. The as-polished micrographs (Figures 4(a)–(b)) clearly show cracks initiating from the inner surface and propagating outward toward the tube wall, consistent with corrosion-assisted degradation originating from the internal environment where condensate and corrosive gases were trapped.

The transverse section (Figure 4(a)) highlights multiple pits acting as micro-stress concentrators, supporting the conclusion that pitting corrosion served as the primary initiation factor for subsequent cracking and material loss. The longitudinal section (Figure 4(b)) exhibits a complex, branched cracking morphology, characteristic of brittle fracture mechanisms associated with stress corrosion cracking (SCC) and hydrogen embrittlement (HE). Localised pitting facilitated passive film rupture, creating preferred paths for SCC crack nucleation and intergranular propagation. These features

correspond with the findings of Scatigno et al. [1] and Yu et al. [12], who reported similar pit-induced crack initiation under chloride exposure and cyclic thermal–mechanical stresses.

The etched micrographs (Figures 4(c)–(d)) provide further insights into crack morphology. The transverse section (Figure 4(c)) displays both intergranular and transgranular cracks, indicative of SCC and HE. This aligns with studies linking environmental (e.g., chlorides/ H_2S) and mechanical (e.g., residual stress) factors to failure progression [1,3,4,10]. The longitudinal section (Figure 4(d)) shows a branched cracking pattern, emphasizing residual stress contributions to corrosion-driven failure. The interplay of pitting corrosion, SCC, and HE underscores the combined role of environmental exposure (moisture, corrosive species) and operational stresses in material degradation.

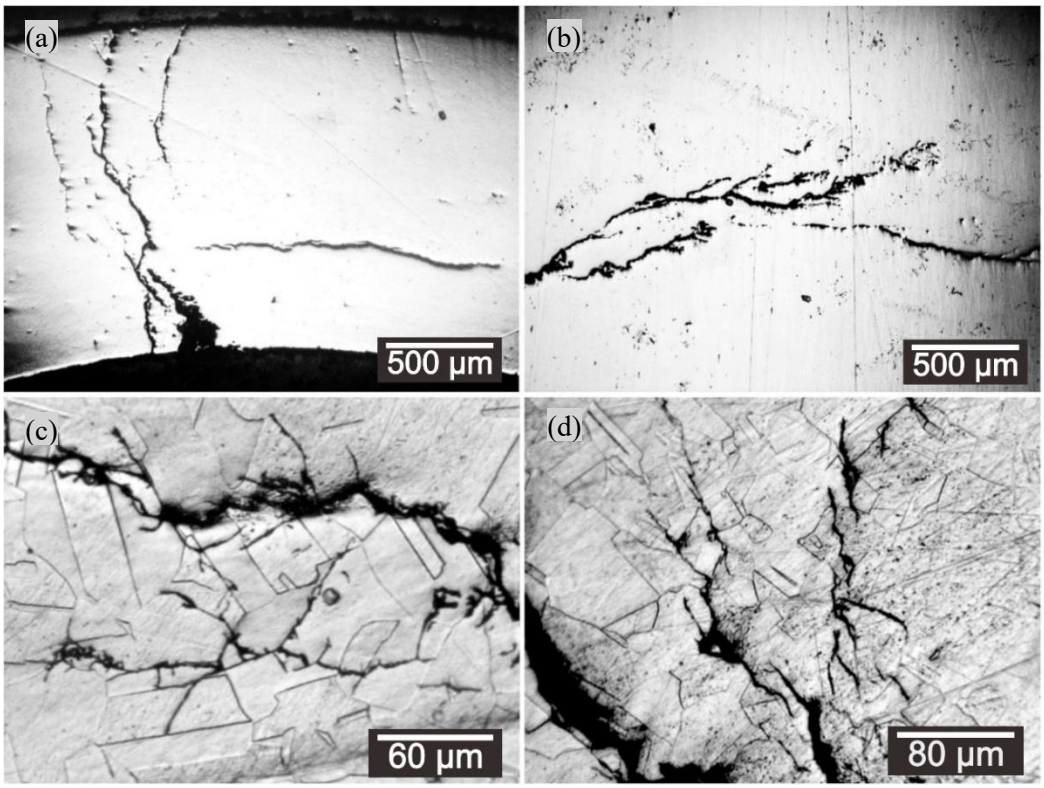

Figure 4: Optical microscope images of the leaked location. (a) Transverse and (b) longitudinal sections (as-polished) show cracks originating from pitting corrosion and SCC. (c) Transverse and (d) longitudinal sections (etched) reveal intergranular and transgranular cracking

3.6 Fractography on Cracked Region

Figure 5 presents scanning electron microscopy (SEM) micrographs of the fracture surface at a pit location, revealing both intergranular and transgranular crack morphologies that provide deeper insight into the failure mechanism. Intergranular cracks follow grain boundaries weakened by hydrogen sulfide (H_2S)-assisted corrosion, a characteristic feature of sulfide stress cracking (SSC) and hydrogen embrittlement (HE) under wet gas environments. The discontinuous and branched nature of these cracks corresponds well with previous studies linking intergranular fracture to hydrogen diffusion and boundary decohesion under corrosive exposure [10]. These findings also corroborate the optical observations in Figure 4(c), which displayed intergranular cracking within the transverse section of the failed tube.

In addition to intergranular features, fine transgranular cracks were observed propagating through the grains, indicating secondary brittle fracture due to cyclic mechanical stresses and thermo-mechanical fatigue during service. This morphology supports the concept of stress corrosion cracking

(SCC) superimposed on hydrogen-related damage, where cracks transition from grain boundaries into the matrix under fluctuating operational loads. Although transgranular cracking was less dominant, its presence highlights the synergistic effect of stress, corrosion, and microstructural weakness in accelerating the overall failure progression of the natural gas fuel tube.

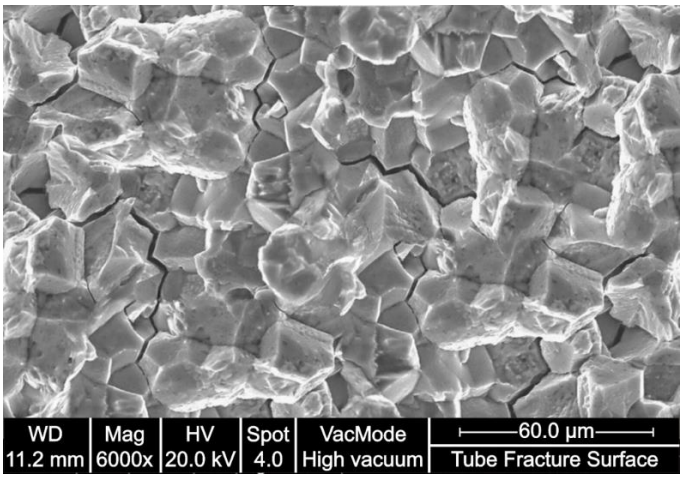

Figure 5: SEM micrographs showing intergranular and transgranular cracking morphologies on the fracture surface of the fuel tube wall

3.7 Failure Mechanism and Rectification Measures

The failure of the fuel supply tubes in the gas turbine system, after approximately 25,000 operational hours, resulted from multiple interacting degradation mechanisms, including condensation-induced corrosion, SCC, SSC, HE, and localised pitting corrosion. Under steady-state operating conditions (20–25 bar, 140 °C), the environment remained relatively dry, minimizing corrosion risks. However, during shutdowns, rapid temperature and pressure drops (to ~1 bar and 25° C) created ideal conditions for condensation. As shown in Figure 6, moisture condensed on internal surfaces, particularly in low-lying regions such as the 6 o'clock position near the bend. The bend geometry exacerbated water pooling, while the coastal environment (250 meters from the seashore) contributed additional moisture via salty air.

Condensation initiated corrosion by destabilising the passive oxide layer. Chloride ions penetrated the oxide layer, creating localised weak points for pitting corrosion. Similarly, H_2S reacted with the oxide layer, forming sulfide compounds that accelerated degradation. Fractographic analysis confirmed intergranular cracking, indicative of SSC, and highlighted the role of HE in accelerating failure. Hydrogen atoms generated from H_2S exposure diffused into the metal lattice under stress, weakening intergranular bonds and reducing ductility. SEM analysis revealed brittle fracture characteristics, supporting findings that HE exacerbates SCC and SSC damage. Chloride ions (up to 5.5 ppm total from HCl, methyl chloride, and ethyl chloride) promoted pitting corrosion by inducing passive film breakdown, creating initiation sites for SCC. Figure 7 schematically illustrates the failure sequence, emphasizing passive film breakdown as the critical first step enabling pitting, followed by SCC/ SSC initiation, crack propagation, and catastrophic failure.

To address these issues, rectification measures must focus on design optimisation, material upgrades, environmental controls, and operational adjustments. Redesigning the tube bend with gradual curvature, smooth transitions, and drainage features minimises condensation and stress concentrations, as recommended in pipeline integrity guidelines. Material selection should prioritize alloys with higher pitting resistance, such as AISI 316L (PREN ~25), Lean Duplex stainless steel (UNS S32101, PREN ~26–28), or Inconel 625 (PREN ~50), to mitigate chloride and H_2S susceptibility. PREN (Pitting Resistance Equivalent Number) quantifies resistance to pitting corrosion, with higher values indicating superior performance in chloride-rich environments.

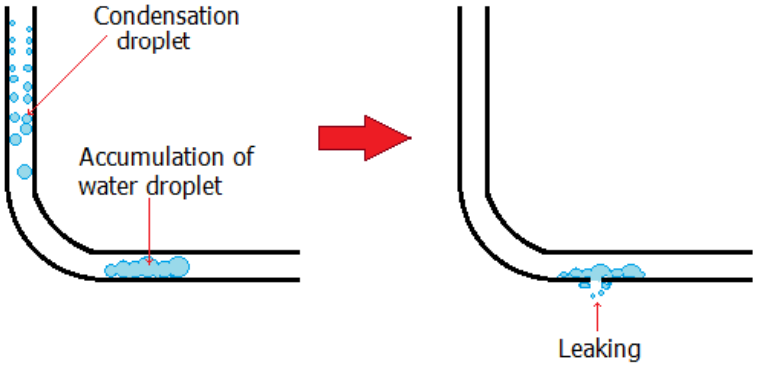

Figure 6: Schematic diagram showing how water droplets from condensation build up and cause the wall tube to leak

Figure 7: Schematic of the failure sequence in fuel tubes, progressing from pitting corrosion to SCC/SSC initiation, crack propagation, and final failure

Operational protocols should incorporate gradual shutdown/ startup procedures. For example, reducing pressure to 5 bar over 30 minutes minimises rapid condensation risks. Maintaining residual pressure during shutdowns further reduces moisture accumulation. Proper insulation of the tubing system stabilises internal temperatures, limiting condensation risks. Environmental controls, such as maintaining relative humidity below 50 % using dehumidifiers, are critical in coastal regions. A structured non-destructive testing (NDT) program, including Phased Array Ultrasonic Testing (PAUT) for sub-surface cracks, Eddy Current Testing (ECT) for surface flaws, and Radiographic Testing (RT) for monitoring crack growth, ensures early detection of degradation. Additionally, applying epoxy-phenolic coatings to internal surfaces enhances corrosion resistance and minimises SCC risks. Frequent inspections in high-risk areas, combined with these strategies, will improve long-term structural integrity and operational reliability.

4. CONCLUSION

The failure of the fuel supply tube was primarily attributed to the tube bend geometry, which promoted water accumulation in adjacent straight sections, leading to condensation-induced corrosion. Rapid temperature and pressure drop during shutdowns accelerated moisture condensation, while H_2S exacerbated sulfide stress cracking (SSC) and hydrogen embrittlement (HE), and chlorides accelerated stress corrosion cracking (SCC) and pitting corrosion. Localised pitting at stress-prone areas served as crack initiation sites, compromising structural integrity. To prevent similar failures, it is essential to implement redesigned tube geometry with gradual curvature and drainage features, adopt corrosion-resistant materials such as AISI 316L, Lean Duplex stainless steel (UNS S32101), or Inconel 625, and enhance inspection protocols (e.g., phased array ultrasonic testing) and operational adjustments (e.g., maintaining residual pressure during shutdowns).

Acknowledgements

The author would like to acknowledge the support from the Fundamental Research Grant Scheme (FRGS) under a grant number of FRGS/1/2022/TK07/UNIMAP/02/101 from the Ministry of Higher Learning Malaysia.

Author Contributions

All authors contributed toward testing, data analysis, drafting, and critically revising the paper and agreed to be accountable for all aspects of the work.

Disclosure of Conflict of Interest

The authors have no disclosures to declare

Compliance with Ethical Standards

The work is compliant with ethical standards.

References

[1] Scatigno, G. G., Ryan, M. P., Giuliani, F. & Wenman, M. R. (2016). The effect of prior cold work on the chloride stress corrosion cracking of 304L austenitic stainless steel under atmospheric conditions. *Materials Science and Engineering. A*. *668*, 20-29.

[2] Okonkwo, P. C., Sliem, M. H., Shakoor, R. A., Mohamed, A. M. A. & Abdullah, A. M. (2017). Effect of temperature on the corrosion behavior of API X120 pipeline steel in H_2S environment. *Journal of Materials Engineering and Performance*. *26(4)*, 3775-3783.

[3] Shah, M., Ayob, M. T. M., Yaakob, N., Embong, Z. & Othman, N. K. (2022). Comparative corrosion behaviour of austenitic 316L and duplex 2205 stainless steels: microstructure and property evolution at highly partial pressure of H_2S. *Corrosion Engineering, Science and Technology*. *57(1)*, 15-31.

[4] Le, Hien, N. T., Dung, N. D., Garfias, L. F. & Hung, T. (2017). Cracking corrosion of low carbon steel in environment with a high concentration of CO_2 and H_2S. *Vietnam Journal of Science and Technology*. *55(5B)*, 210-216.

[5] Popescu, C. & Gabor, M. R. (2021). Quantitative analysis regarding the incidents to the pipelines of petroleum products for an efficient use of the specific transportation infrastructure. *Processes*, *9(9)*, 1535.

[6] Ma, Z., Wang, X., Yang, J., Wang, W., Shao, W. & Jiang, X. (2021). Acid corrosion analysis in the initial condensation zone of a H_2O/CO_2 turbine. *Energies*. *14(11)*, 3323.

[7] Huang, F., Zhou, Z. J., Hua, X., Chen, G. F. & Zhou, X. Z. (2016). Effect of thermal gradient on the thermomechanical fatigue behavior of thermal barrier coating system. In Proceedings of the 4th 2016 International Conference on Material Science and Engineering (ICMSE 2016), Guangzhou, China, 24-26 June 2016.

[8] Radhakrishnan, G., Breaz, D., Al Khusaibi, S. S., Al Subaihi, A. J., Al Ismaili, A. A. Z., AlMaani, A. M. & Karthikeyan, K. R. (2023). Experimental and numerical study on the influence of stress concentration on the flexural stability of an aluminium hollow tube. *Materials*. *16(4)*, 1492.

[9] Ajayi, F. O. & Lyon, S. (2023). Mitigation of top-and bottom-of-the-line CO_2 corrosion in the presence of acetic acid (II): Inhibition using azole derivatives. *Materials and Corrosion*. *74(8)*, 1208-1216.

[10] Elkhodbia, M., Negi, A., Mubarak, G., Barsoum, I. & AlFantazi, A. (2023). Review on sulfide stress cracking in sour service for OCTG and recent advances in modeling of hydrogen-assisted fracture. *Geoenergy Science and Engineering*. *230(10)*, 212174.

[11] Fonseca, D., Tagliari, M. R., Guaglianoni, W. C., Tamborim, S. M. & Borges, M. F. (2024). Carbon dioxide corrosion mechanisms: historical development and key parameters of CO_2-H_2O systems. *International Journal of Corrosion*, *2024(1)*. 5537767.

[12] Yu, L., Chang, Y., Yi, L., Chen, Y., Yang, C. & Gao, J. (2020). Analysis method of brittle failure probability of steel members. In Proceedings of the 2nd International Conference on Civil Architecture and Energy Science (CAES 2020), Changchun, China, 20–22 Mar 2020.

[13] Hamdan, H., Alsit, A., Al Tahhan, A. B., Mughieda, O., Mourad, A. H. I., Shehadeh, M. A. & Alkhedher, M. (2024). Prognosis methods of stress corrosion cracking under harsh environmental conditions. *Heliyon*. *10(3)*,e25276.

[14] Latypova, D. & Latypov, O. (2021). Method of Investigation of Local Corrosion Processes on Samples from Clad Steel. In Proceedings of the Proceedings of the Corrosion in the Oil & Gas Industry 2020, St. Petersburg, Russia, 14–16 Dec 2020.

[15] Alhede, A., Dijkstra, J., Robuschi, S., Tengattini, A. & Lundgren, K. (2023). A two-stage study of steel corrosion and internal cracking revealed by multimodal tomography. *Construction and Building Materials*. *394*, 132187.